# Modeling Validation and Simulation of an Anode Supported SOFC including Mass and Heat Transport, Fluid Flow and Chemical Reactions

Andersson, Martin; Yuan, Jinliang; Sundén, Bengt; Li, Ting Shuai; Wang, Wei Guo

*Published in:*
ASME 2011 9th International Conference on Fuel Cell Science, Engineering and Technology. Collocated with ASME 2011 5th International Conference on Energy Sustainability, FUELCELL 2011

*DOI:*
10.1115/FuelCell2011-54006

2011

Appendix to Dissertation: *Solid Oxide Fuel Cell Modeling at the Cell Scale - Focusing on Species, Heat, Charge and Momentum Transport as well as the Reaction Kinetics and Effects* by Martin Andersson, Department of Energy Science, Lund University, 2011, ISBN 978-91-7473-180-4.

# Paper VII

This paper has been published in:

*Proceedings of the ASME 9th International Fuel Cell Science, Engineering & Technology Conference, Washington, DC, USA,*
ASME ESFuelCell2011-54006, 2011.

**Proceedings of the ASME 2011 Ninth International Fuel Cell Science, Engineering and Technology Conference**
**FuelCell2011**
**August 7-10, 2011, Washington, DC, USA**

# ESFuelCell2011-54006

# MODELING VALIDATION AND SIMULATION OF AN ANODE SUPPORTED SOFC INCLUDING MASS AND HEAT TRANSPORT, FLUID FLOW AND CHEMICAL REACTIONS

**Martin Andersson** **Jinliang Yuan** **Bengt Sundén**
Department of Energy Sciences, Faculty of Engineering,
Lund University, Box 118, 221 00 Lund, Sweden

**Ting Shuai Li** **Wei Guo Wang**
Division of Fuel Cell and Energy Technology, Ningbo Insitute of Material Technology & Engineering,
Chinese Academy of Sciences, 519 Zhuangshi Road, Ningbo, 315201, China

## ABSTRACT

Fuel cells are electrochemical devices that directly transform chemical energy into electricity, which are promising for future energy systems, since they are energy efficient and, when hydrogen is used as fuel, there are no direct emissions of greenhouse gases. The cell performance depends strongly on the material characteristics, the operating conditions and the chemical reactions that occur inside the cell. The chemical- and electrochemical reaction rates depend on temperature, material structure, catalytic activity, degradation and the partial pressures for the different species components. There is a lack of information, within the open literature, concerning the fundamentals behind these reactions. Experimental as well as modeling studies are needed to reduce this gap.

In this study experimental data collected from an intermediate temperature standard SOFC with $H_2/H_2O$ in the fuel stream are used to validate a previously developed computational fluid dynamics model based on the finite element method. The developed model is based on the governing equations of heat and mass transport and fluid flow, which are solved together with kinetic expressions for internal reforming reactions of hydrocarbon fuels and electrochemistry. This model is further updated to describe the experimental environment concerning cell design. Discussion on available active area for electrochemical reactions and average ionic transport distance from the anodic- to the cathodic three-phase boundary (TPB) are presented. The fuel inlet mole fractions are changed for the validated model to simulate a $H_2/H_2O$ mixture and 30 % pre-reformed natural gas.

*Keywords:* *SOFC, Modeling, Validation, Active Area, Ionic Transport Distance, COMSOL Multiphysics*

## INTRODUCTION AND PROBLEM STATEMENT

Fuel cells (FCs) are promising due to advantages of higher efficiency and lower emissions of $SO_X$, $NO_X$ and $CO_2$ than conventional power generation [1]. The solid oxide fuel cell (SOFC) is a high temperature fuel cell, which operates at 600-1000 ºC [2]. This temperature allows SOFCs to operate with different types of fuels from both fossil and renewable sources. It opens a way for an easier transition from conventional power generation with hydrocarbon based fuels to fuel cells with possibility for different fuels, especially SOFCs. Due to the increasing global awareness of that energy usage affects the environments, the interest of renewable energy has increased. SOFCs are generally more tolerant to contaminants than other fuel cells and the possibility to internally (as well as externally) reform the fuel make them interesting for renewable energy resources [1].

Numerical results of SOFC models are only approximations of real conditions and the validation is an important and necessary step in the development of reliable and accurate computational models. A range of validity can be established between the developed model and experimental

 

data. When poor agreement is found between experiments and computations, the task is to understand where the errors come from, the modeling or the experimental work, for the objective to make better models or perform better experiments. It should be noted that CFD (computational fluid dynamics) models makes it possible to reduce the amount of experimental tests needed for cell development, only a limited amount of tests is required to validate the accuracy of the model. This means that the development cost can be decreased [3].

The aim of this paper is to validate a previously developed model, for an intermediate temperature anode-supported SOFC, with the scale of single unit-cell [2,5]. A NIMTE (Ningbo Insitute of Material Technology & Engineering) standard cell is used, as described in the next section.

The global reactions that take place within a SOFC, using hydrogen as fuel, can be described as: oxygen is reduced at the cathodic three-phase boundary (TPB), eqn. (1). The oxygen ions are transported through the electrolyte, but the electrons are prevented to passing through the electrolyte. The electrochemical reactions between hydrogen and oxygen ions, eqn. (2), take place in the anodic TPB [6-7].

$$\frac{1}{2}O_2 + 2e^- \Leftrightarrow O^{2-} \quad (1)$$

$$H_2 + O^{2-} \Leftrightarrow H_2O + 2e^- \quad (2)$$

When a fuel containing methane or carbon monoxide, i.e., the main components of natural gas is supplied, the reforming takes place within the anode. Methane is reformed with steam (eqn. (MSR, 3)). Carbon monoxide can be oxidized in the electrochemical reaction, and also react with water (eqn. (WGSR, 4)) [6]. The reactions described here are the overall ones, more detailed reaction mechanisms can be found in [7].

$$CH_4 + H_2O \Leftrightarrow 3H_2 + CO \quad \text{(MSR, 3)}$$

$$CO + H_2O \Leftrightarrow H_2 + CO_2 \quad \text{(WGSR, 4)}$$

## EXPERIMENTAL STUDY ON THE NIMTE STANDARD CELL

Experiments were carried out for a typical intermediate temperature anode-supported SOFC manufactured by Division of Fuel Cell and Energy Technology at NIMTE, and a SEM image is shown in Figure 1. The cell consists of a 400 μm thick Ni (40%) / YSZ (60%) anode substrate and an active anodic layer of 15 μm, where the electrochemical reactions occur. The electrolyte is a 10 μm thick layer of YSZ. The cathode consists of a 20 μm thick active layer of LSM/YSZ and a buffer layer of 50 μm LSM. Note that the anode active- and support layers have the same material composition, and the interface may not be very distinct. The major function of the anodic active layer is for the electrochemical reactions at TPBs, while the support layer should enable internal reforming reactions. It is a fact that a fine porous microstructure with a high surface area may lead to a decreased mechanical strength. The anode is often used as the mechanical support for the cell, i.e., this can be problematic. Since the active region in the anode where the electrochemical reactions take place does not extend too long from the anode–electrolyte interface, a graded porosity can be used to maximize the amount of TPB in the active region. The high mechanical strength is maintained for the rest of the anode which is used primarily as the cell support and for internal reforming reactions, when hydrocarbons are supplied as fuel [8].

The anodic porosity measured is 28 %. The fuel- and air flows are arranged as counter-flows. For the testing, a fuel flow rate of 800 sccm and an air flow rate of 2000 sccm are used. The single cell sample has dimensions of 5*5.8 $cm^2$, with an active area of 4*4 $cm^2$. An alumina testing house is used, where the cell temperature is kept constant during the tests, i.e., 750 °C for this case. Voltage probes are placed on the surface of the anode- and cathode support. The measurement data from the cell testing are presented and compared with our model predictions in the validation section.

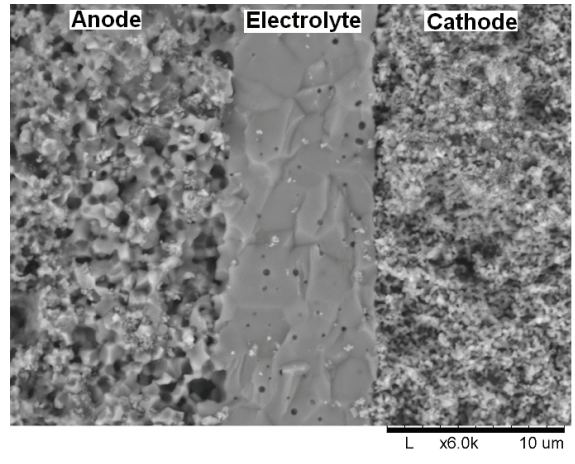


**Figure 1: A SEM image of a tested SOFC cross section, with (from left to right) anode active layer, electrolyte and cathode active layer.**

## MATHEMATICAL MODEL

A two-dimensional (2D) model for an anode-supported SOFC is developed and implemented in the commercial software, COMSOL Multiphysics (version 3.5a). Equations for momentum-, mass- and heat transport are solved simultaneously. As our model is defined in 2D only, i.e., the calculation is for a domain at the mid-plane of a unit cell. In reality the current density will be higher in the middle of the electrodes. The model is in this paper validated against a 1D

(flow direction) current density, i.e., the y-direction is neglected. The geometry is defined in Table 1 and a sketch of the investigated cell can be seen in Figure 2. The thickness of the electrodes, electrolyte and interconnect are updated (compared to our previous model [2,4-5]) to describe a standard intermediate temperature SOFC developed at NIMTE. Note that Figure 2 is not to scale.

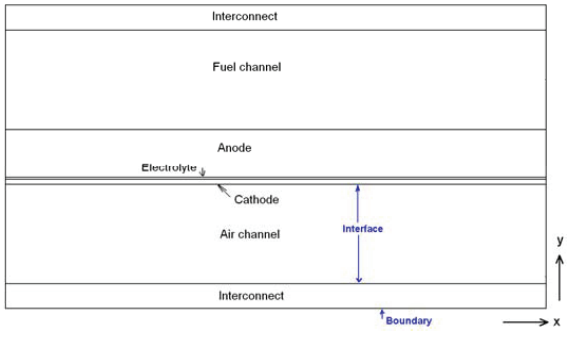


**Figure 2: Sketch of an anode-supported SOFC, not to scale.**

**Table 1: Cell geometry**

| Cell Component | Thickness (τ) |
|---|---|
| Cell length | 0.04 / 0.1 m [1] |
| Fuel channel height | 1 mm |
| Air channel height | 1 mm |
| Anode thickness | 415 μm [2] |
| Cathode thickness | 70 μm [3] |
| Electrolyte thickness | 10 μm |
| Interconnect thickness | 300 μm |

## Momentum transport

The gases flow inside the fuel cell components, such as in the air and fuel channels, and in the porous electrodes. The Darcy-Brinkman equation is introduced and solved for the gas flow in the fuel and air channels, and in the porous materials simultaneously [9-10]. The Darcy-Brinkman equation (eqn.(5)) is transformed into the standard Navier-Stokes equation when ($\kappa \to \infty$) and ($\varepsilon_p = 1$), and into the Darcy equation as ($Da \to 0$). $Da$ is the Darcy number. The derivation of Navier-Stokes equation and Darcy equation from Darcy-Brinkman equation can be found in [9].

$$\left(\frac{\mu}{\kappa}+\rho\cdot\nabla \mathrm{u}\right)\mathrm{u}-\nabla\left[-p+\frac{1}{\varepsilon_p}\left\{\mathbf{T}-\left(\frac{-2}{3}\cdot\mu\right)(\nabla \mathrm{u})\right\}\right]=\mathbf{F} \qquad (5)$$

where $\mathbf{F}$ is the volume force vector, $\kappa$ is the permeability of the porous medium, $\varepsilon_p$ the porosity, $\mu$ the dynamic viscosity, u the velocity vector and $\mathbf{T}$ the viscous stress tensor $\left(\mathbf{T}=\mu\left(\nabla \mathrm{u}+(\nabla \mathrm{u})^T\right)\right)$. The density and viscosity for the participating gas mixtures are dependent on local mole fraction and temperature, as described in [2,5]. The gas inlet velocities are defined as a laminar flow profile. The average velocities for the validation are based on the measured flow rates by taking into account the fuel- and oxygen utilization, respectively. The outlets are defined as pressure (1 atm).

## Mass transport

In the porous material, there are two kinds of mass diffusion mechanisms; molecular and Knudsen diffusions. The molecular diffusion (collisions between gas molecules) is significant in the case of large pores, whose size is much bigger than the mean free path of the diffusion gas molecules [11-12]. For a multi-component gas mixture system, the diffusion coefficients are calculated by the expressions in [13], based on bi-component coefficients of the gases. Knudsen diffusion is important when the mean free path is in the same order or bigger than the pore size, and molecules collide with the solid walls more often than with other molecules**.** At the SOFC operating temperature of around 1000 K, the mean free path of these gas components is about 0.2-0.5 μm. In this study, the radius of pores is assumed as 0.34 μm, which is of the same order as the mean free path. In other words the Knudsen diffusion should be included in the SOFC models. The Knudsen diffusion coefficient of the component $i$ with the component $j$ in a gas mixture, $D_{k,ij}$, is calculated based on the free molecule flow theory, as described in [14]:

$$D_{k,ij}=\frac{2}{3}\cdot r_e\cdot\sqrt{\frac{8\cdot \mathrm{R}\cdot T}{\pi\cdot M_{ij}}} \qquad (6)$$

where $r_e$ is the effective radius of the pores, R the universal gas constant. In the porous media, there is an increased diffusion length due to the tortuous paths of connected real pores, and the coefficients are usually corrected by porosity $\varepsilon$ and tortuosity $\tau$ [12,14]:

$$D_{eff,ij}=\frac{\varepsilon}{\tau}\cdot\left(\frac{D_{i,j}\cdot D_{k,ij}}{D_{i,j}+D_{k,ij}}\right) \qquad (7)$$

Equation (8) is used to describe the mass transport phenomena for each gas component inside the cell [10] and solved for the fuel- and air channels and the electrodes.

$$\nabla\left(-\rho\cdot w_i\sum_{j}^{n}D_{eff,ij}\cdot\nabla x_j+\left(x_j-w_j\right)\frac{\nabla p}{p}\cdot \mathrm{u}-D_i^T\cdot\frac{\nabla T}{T}\right)+\rho\cdot \mathrm{u}\cdot\nabla w_j=S_i \qquad (8)$$

where $w$ is the mass fraction, $x$ the molar fraction, $n$ the number of species and $D_i^T$ the thermal diffusion coefficient. $S_i$, the

[1] The cell length in the experimental cell used for validation is 4 cm. In the final model the cell length equals 10 cm.

[2] The anode consists of a 400 μm thick support layer and a 15 μm functional layer.

[3] The cathode comprises of a 50 μm thick support layer and a 20 μm functional layer.

source term by the chemical reactions, is defined for the internal reforming reactions.

Two approaches for defining the electrochemical reactions can be found in the literature, either as source terms in the governing equations [14-15] or as interface conditions defined at the electrode/electrolyte interfaces [16-17]. The later concept is employed in this study, because the thickness of the active layer is relatively thin [16-17]. This limitation will be released later in our future studies. The boundary conditions for the mass transport equation are defined as mass fractions for the gas channel inlets and the outlets are defined as convective flux.

### Heat transport

The temperature distribution is calculated separately for the gas phase (in air and fuel channels and electrodes) and for the solid phase (interconnects, electrodes and electrolyte). Heat is transferred between the phases at the channel walls and in the porous electrodes. The general heat conduction equation is used to calculate the temperature distribution for the solid materials, i.e., electrolyte, interconnect and electrodes [10]:

$$\nabla\left(-k_s \cdot \nabla T_s\right) = Q_s \tag{9}$$

where $k_s$ is the thermal conductivity of the solids, $T_s$ the solid temperature and $Q_s$ the heat source (heat transfer between the solid and gas phases, and heat generation due to ohmic polarization). Heat generation due to electrochemical reactions, mole fraction and activation polarization are simplified and defined as interface conditions, such as for the mass transport.

The temperature distribution for the gas mixtures in the fuel and air channels and in the porous electrodes is calculated as [10]:

$$\nabla\left(-k_g \cdot \nabla T_g\right) = Q_g - \rho_g \cdot c_{p,g} \cdot \mathrm{u} \cdot \nabla T_g \tag{10}$$

in which $c_{p,g}$ is the gas phase specific heat (dependent on temperature and mole fraction, as described in [5]), $T_g$ the temperature in the gas phase, and $Q_g$ the heat transfer between the gas and solid phases and the heat consumption due to internal reforming reactions.

The heat transfer between the gas- and solid phase, in the electrodes, depends on the temperature difference and the particle surface area ratio as [18]:

$$Q_g = h_v \cdot \left(T_g - T_s\right) = AV \cdot h_{s,g,por} \cdot \left(T_g - T_s\right) \tag{11}$$

in which $h_v$ is the volume heat transfer coefficient and $AV$ the surface area ratio, which is used for heat transfer between the solid- and gas phase. The heat transfer coefficient ($h_{s,g,por}$) is calculated as described in [19]. Note that the surface area for heat transfer is higher than that for chemical reactions, because not all the available surface is covered with active nickel catalyst. The specific heat and the thermal conductivity of the gas phase depend on the local temperature and the mole fraction, as described in [2,5].

The inlet gas temperature is defined by the operating temperature and the outlet is defined as a convective flux. The boundaries at the top and the bottom of the cell are defined by symmetries, since it is assumed that the cell is surrounded by other cells with the same temperature distribution. The heat flux between the electrodes/interconnect and gas channels are specified at two channel walls, located opposite to each other, with a constant Nusselt number (4.094) from [20], based on the fully developed flow for a square duct (aspect ratio is 1 for both channels).

### Electrochemical reactions

The charge transfer equations are not solved in this study, however the effects from ohmic-, concentration- and activation polarization losses are included in the equations for heat transport. The electromotive force (reversible open-circuit voltage, $E^{OCV}$) is determined by the difference in the thermodynamic potentials of the electrode reactions [21-23]. When a hydrogen-steam mixture is used as fuel, it can be calculated by the Nernst equation [23]:

$$E^{OCV} = E^0 - \frac{\mathrm{R} \cdot T}{2 \cdot \mathrm{F}} \cdot \ln\left(\frac{p_{H_2O}}{p_{H_2}\sqrt{p_{O_2}}}\right) \tag{12}$$

$$E^0 = 1.253 - 2.4516 \cdot 10^{-4} \cdot T \tag{13}$$

where $E^0$ is the temperature dependent open circuit voltage at standard pressure and $p_i$ the partial pressure, at the TPB, in atm.

It should be noted that eqns. (12)-(13) are only valid for pure hydrogen-steam mixtures. The electromotive force for only carbon monoxide or methane as fuel is presented in eqns. (14)-(15), respectively. $E^0$ for carbon monoxide decreases with increased temperature, but it is not temperature dependent for methane, due to a constant molar number of products and reactants [21-22]. In this study only eqns. (12)-(13) are used to calculate the electromotive force, i.e., it is assumed that methane and carbon monoxide reacts with steam and only $H_2$ participates in the electrochemical reactions. For this case of the mixture of $H_2$, $CH_4$ and CO presented the Nernst equation may not be applicable. Our aim is to release this limitation in future studies.

$$E_{CO}^{OCV} = E_{CO}^0 - \frac{\mathrm{R} \cdot T}{2 \cdot \mathrm{F}} \cdot \ln\left(\frac{p_{CO_2}}{p_{CO}\sqrt{p_{O_2}}}\right) \tag{14}$$

$$E_{CH_4}^{OCV} = E_{CH_4}^0 - \frac{\mathrm{R} \cdot T}{8 \cdot \mathrm{F}} \cdot \ln\left(\frac{p_{CO_2} \cdot {p_{H_2O}}^2}{p_{CH_4} \cdot {p_{O_2}}^2}\right) \tag{15}$$

Due to internal resistance and overpotential losses the actual voltage ($E$) becomes less than the open-circuit voltage. $E$ can be expressed as [23]:

$$E = E^{OCV} - \eta_{act} - \eta_{ohm} - \eta_{conc} \tag{16}$$

where $\eta$ are the respectively polarization losses.

Ohmic polarization occurs due to resistance of the flow of ions in the electrolyte and electrical resistance in the electrodes. The electrodes and electrolyte are heated due to this effect [23-24]:

$$Q_{ohm} = \frac{i \cdot \eta_{ohm}}{\tau} \tag{17}$$

$$\eta_{ohm} = \left( \frac{\tau_a}{\sigma_a} + \frac{\tau_{el}}{\sigma_{el}} + \frac{\tau_c}{\sigma_c} \right) \cdot i \tag{18}$$

where $\tau$ is the component thickness. The electronic/ionic conductivities ($\sigma$) are calculated as described in [23].

Heat generation due to the electrochemical reactions and concentration- and activation polarization losses are defined at the electrodes/electrolyte interfaces:

$$-\mathrm{n} \cdot \left(-k \nabla T\right)- = q_0 \tag{19}$$

$$q_0 = q_r + q_{losses} = -i \cdot \left( \frac{T \cdot \Delta S_r}{n_e \cdot \mathrm{F}} + \eta_{act,e} + \eta_{conc,e} \right) \tag{20}$$

where $q_o$ is the total heat generation, $q_r$ the heat generated inside the cell due to change in enthalpy and $q_{losses}$ the heat generated due to concentration- and activation polarization losses inside the cell. The amount of heat generated due to electrochemical reactions can be calculated as [25]:

$$q_r = -T \cdot \Delta S_r \cdot \dot{n} = -\Delta S_r \frac{T \cdot i}{n_e \mathrm{F}} \tag{21}$$

$$\dot{n} = \frac{i}{n_e \mathrm{F}} \tag{22}$$

where $\dot{n}$ is the molar flux density [mol/(m$^2$s)] and $\Delta S_r$ entropy change of the reaction (-50.2 J/(K mol)), calculated from data in [26]. The concentration polarizations are specified as [23]:

$$\eta_{conc,a} = \frac{\mathrm{R}T}{n_{e,a} \mathrm{F}} \ln\left( \frac{p_{H_2O,TPB} \cdot p_{H_2,b}}{p_{H_2,TPB} \cdot p_{H_2O,b}} \right) \tag{23}$$

$$\eta_{conc,c} = \frac{\mathrm{R}T}{n_{e,c} \mathrm{F}} \ln\left( \frac{p_{O_2,b}}{p_{O_2,TPB}} \right) \tag{24}$$

where $p_{i,TPB}$ stands for the partial pressure at three phase boundary (TPB) and $p_{i,b}$ the partial pressure at the interface between gas channel and electrode. The chemical reactions involve energy barriers (i.e., activation polarization) which must be overcome by the reacting species.

The activation polarization can be considered as the extra potential needed to overcome the energy barrier of the rate-determining step to a value that the reaction proceeds at a desired rate [27]:

$$\eta_{act,e} = \frac{2\mathrm{R}T}{n_e \mathrm{F}} \sinh^{-1}\left( \frac{i_e}{2 \cdot i_{0,e}} \right) \tag{25}$$

$$i_{0,e} = \frac{\mathrm{R}T}{n_e F} k''_e \cdot \exp\left( \frac{-E_e}{\mathrm{R}T} \right) \tag{26}$$

where $i_{0,e}$ is the exchange current density. The pre-exponential factor ($k''$) is $2.35 \cdot 10^{11}$ $\Omega^{-1}$m$^{-2}$ for the cathode and $6.54 \cdot 10^{11}$ $\Omega^{-1}$m$^{-2}$ for the anode, respectively. The activation energy ($E$) is 137 kJ/mol for the cathode and 140 kJ/mol for the anode [23].

### Internal reforming reactions

Sufficient activity for the reforming reactions is provided inside the SOFC anode [28]. Reaction kinetics from [29] for the steam reforming, eqn. (MSR, 3), (an expression dependent on the active area to volume ratio) and from [30] for the water-gas shift, eqn. (WGSR, 4), reactions are used to calculate the reaction rates in this work. Other global kinetic models can be found in [31-32]. The catalytic methane steam reforming reaction occurs at the surfaces of the nickel catalysts and is specified as [29,33]:

$$r_r = AV \cdot \begin{pmatrix} 943 \cdot \exp\left( \frac{-225 \cdot 10^3}{R \cdot T} \right) \cdot p_{CH_4} p_{H_2O} \\ -7.74 \cdot 10^{-9} \cdot \exp\left( \frac{-1937}{R \cdot T} \right) \cdot p_{CO} p_{H_2}^3 \end{pmatrix} \tag{27}$$

where $p_i$ is the partial pressure of gas species $i$, $T$ the temperature, $r$ the reaction rate and $AV$ the active surface area to volume ratio. Equation (27) origins from the experiments performed at Research Centre Jülish, and the anode material consists of Ni−8YSZ substrate [33].

The range for the AV (related to catalytic kinetic reactions) varies in the literature between $1 \cdot 10^5$ m$^2$/m$^3$ [34] and $2.2 \cdot 10^6$ m$^2$/m$^3$ [29] for SOFC anodes. The measured specific surface area for Ni/YSZ material developed for SOFC anodes is $70 \cdot 10^6$ m$^2$/m$^3$ in [35]. Note that not all the surfaces are available for the catalytic reactions, due to the distribution of catalyst, unavailable pores and mass transfer limitations among others. An AV of $2.2 \cdot 10^6$ m$^2$/m$^3$, corresponding to 3.1 percent of the total Ni/YSZ specific area to volume ratio, is used in this work.

The trend for the FC development in recent years has been in the direction of employing smaller pores to get a larger AV.

Based on the global scheme for the anode, the expression for the catalyzed water-gas shift reforming reaction eqn. (WGSR, 4) in [30] has been selected in this study:

$$r_s = k_{sf} \cdot \left( p_{H_2O} p_{CO} - \frac{p_{H_2} p_{CO_2}}{K_{ps}} \right) \quad (28)$$

The rate constant ($k_{sf}$) and the equilibrium constant ($K_{ps}$) are temperature dependent expressions calculated from the experimental data, as described in [30].

The source terms $S_i$ (implemented in the Maxwell-Stefan equations for the gas species, eqn. (8)), due to the catalytical reforming reactions and the heat generation/consumption due to the reforming reactions, is specified in [4-5].

## VALIDATION

The electrochemical reactions, within the anode as well as within the cathode, occur at the TPBs, i.e., the sites which is connected to the ionic-, electronic- as well as gas phase. The reaction rate decreases drastically as the distance from the electrolyte/electrode interphase increases [16-17]. Two approaches are available to describe the electrochemical reactions in a CFD model, either as a source term (volume), or as an interphase condition (cross-sectional area, x- and z directions). When the concept with the source term is applied, the active thickness of the anode (h) and the active area for electrochemical reactions per volume (AV) need to be defined, as can be seen in Figure 3. For the concept with the interface condition, as applied in this study, the factor "f" is introduced. It is calculated by validating a theoretical model with the experiments. It can be described as the active area available for electrochemical reactions divided by the x-z cross sectional area. To compare the two concepts, f = AV • h.

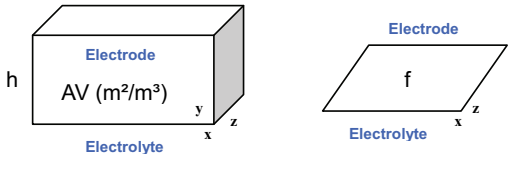


**Figure 3: Sketch over the concepts (source term, to the left, and interface condition, to the right) to define active area for the electrochemical reactions**

The test results from the NIMTE standard cell experiments are presented in Figure 4. The cell testing is conducted at 750 °C. It is assumed that the temperature is constant within the cell, since the cell is placed in a heated oven. In Figure 4, the geometric dimensions and the active area available for electrochemical reactions (Figure 3) are updated, in which f is 0.60. The agreement is not very good at high currents, where the model predicts higher currents compared to the experiments. It would be possible to validate the model to a constant voltage, and an accurate agreement with the experiments would be reached, however the purpose of this validation is to develop a model valid for a range of cell voltages.

The agreement between the modeling and experimental results is improved, when the ohmic losses are increased (by a factor of two) to consider that the electrochemical reactions take place in a region away from the electrode/electrolyte interface, i.e., to consider the distance that the oxygen ions need to be transported, from the air side to the fuel side of the cell. This transport distance factor is ignored in our previous model since the charge transport equations are not included. The agreement between the experiments and the model is improved, as seen in Figure 4 and f is 0.88. Note that the agreement is good when the voltage varies between 0.6 and 1.0 V.

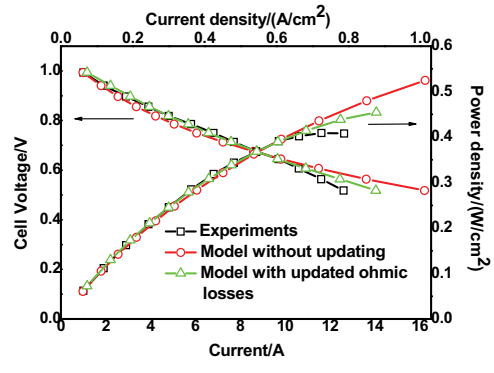


**Figure 4: Comparison between the measured and predicted performance of single SOFC cell.**

## SIMULATION RESULTS FROM VALIDATED MODEL

As a first step simulation results with a hydrogen-steam mixture ($x_{H2}$ : $x_{H2O}$ = 0.90 : 0.10) are presented, i.e., at the conditions similar to the experiments. A base condition is assumed that the cell voltage is 0.7 V, the oxygen utilization 18 % and the fuel utilization 70 %. Co-flow is applied in this model. The inlet temperature for the air and fuel flows are adjusted to make sure that the cell average temperature is 750 °C, the one used in the experimental work and for the validation.

The anode current density along the flow direction is presented in Figure 5. The current density increases along the main flow direction as the temperature rises and this increase eases as the mole fraction of hydrogen within the anode decreases.

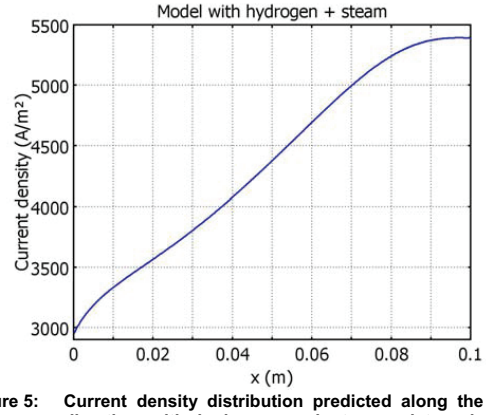


**Figure 5: Current density distribution predicted along the flow direction with hydrogen and steam mixture in fuel stream.**

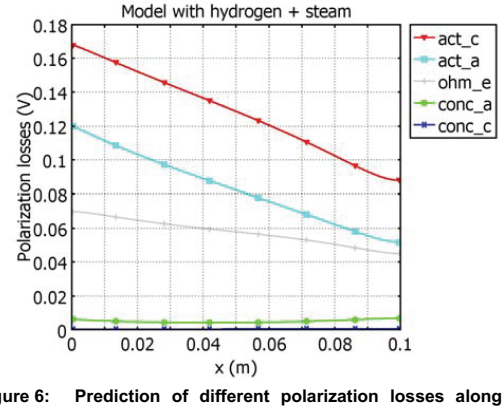


**Figure 6: Prediction of different polarization losses along the flow direction with hydrogen and steam mixture in fuel stream.**

A future step could adjust the active area, porosity and/or particle size along the flow direction to adequate the current density. The polarization losses within the cell are presented in Figure 6. The activation polarization loss corresponds to a majority of the losses and is larger in the cathode compared to the anode and it decreases as the temperature increases. Also the ohmic losses within the electrolyte decreases along the flow direction as the temperature increases. The polarization loss due to concentration differences across the anode is small for these conditions at the inlet and of the fuel composition.

The fuel inlet conditions are further modified as 30% pre-reformed natural gas, as defined by IEA and frequently found in the open literature, i.e, $x_{H2} : x_{CH4} : x_{CO} : x_{H2O} : x_{CO2} = 0.2626 : 0.171 : 0.0294 : 0.4934 : 0.0436$ [31]. The voltage, oxygen and fuel utilization and average temperature are the same as the case above.

The anode current density along the flow direction (Figure 7) increases initially as the temperature increases. It decreases as the mole fraction of hydrogen decreases. Note that the current density is significantly lower for this case with 30 % pre-reformed natural gas, compared to the case with a hydrogen-steam mixture (Figure 5).

The polarization losses are presented in Figure 8. It should be noted that the reversible open-circuit voltage is lower for the case with pre-reformed natural gas, since the mole fraction of hydrogen is lower and the mole fraction of steam is higher, compared to the hydrogen-steam mixture (Figure 6). This gives a lower total amount of polarization losses, since the cell voltage is defined to the same constant value (0.7 V). The same trend for the polarization losses are found, except for the anode concentration polarization, a lower mole fraction of hydrogen give higher losses, due to the fact that hydrogen is consumed in the electrochemical reactions.

The molar fraction of hydrogen (Figure 9) decreases due to the electrochemical reactions at the anode/electrolyte interface and increases due to the reforming reactions (MSR+WGSR) within the anode. The effect of Knudsen diffusion (collisions between gas molecules and the porous walls) is significant. Large mole fraction gradients can be observed through the cell (y-direction). Water (Figure 10) is generated due to the electrochemical reactions and consumed in the reforming reactions (MSR+WGSR). The mole fraction of water reaches its highest value at the anode/electrolyte interface and increases along the flow direction. Carbon monoxide (Figure 11) is generated in the eqn. (MSR, 3) and consumed in the water-gas shift reaction (WGSR). The mole fraction gradient through the anode (y-direction) is large and the smallest mole fraction is found at the TPB and decreasing along the flow direction. Carbon dioxide (Figure 12) is generated in the WGSR and transported through the anode and out of the cell with the exhaust flow stream. A distinct mole fraction gradient can be seen through the anode (y-direction). The highest mole fraction is found close to the gas outlet at the TPB.

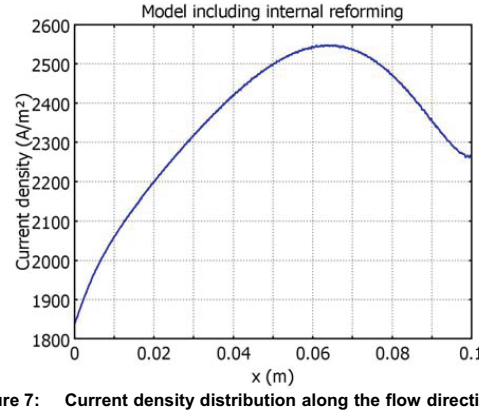


**Figure 7: Current density distribution along the flow direction for the model with natural gas in the fuel stream.**

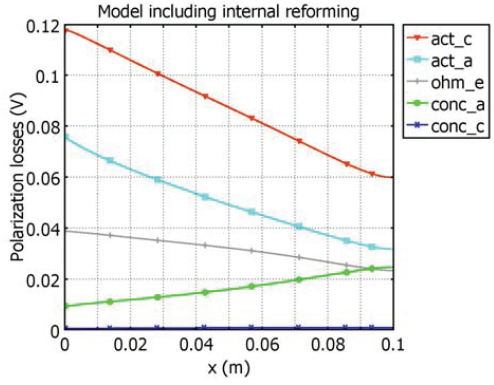


**Figure 8: Different polarization losses along the flow direction for the model with natural gas in the fuel stream.**

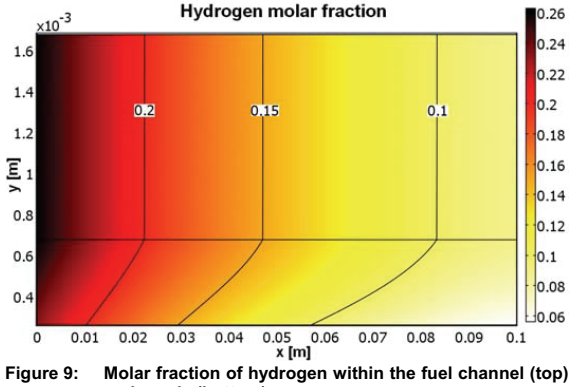


**Figure 9: Molar fraction of hydrogen within the fuel channel (top) and anode (bottom).**

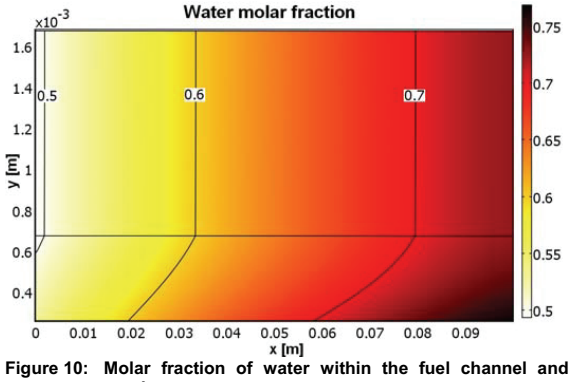


**Figure 10: Molar fraction of water within the fuel channel and anode.**

Methane (Figure 13) is consumed in the eqn. (MSR, 3). Also for methane a clear mole fraction gradient can be observed

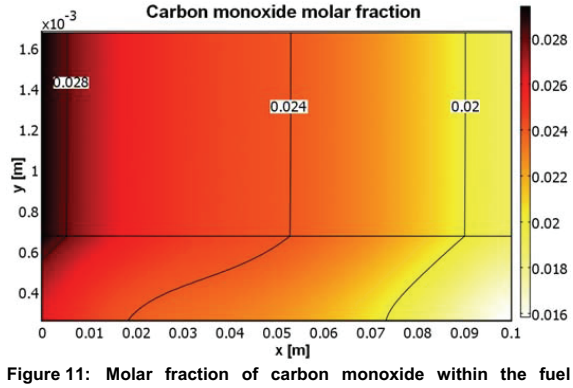


**Figure 11: Molar fraction of carbon monoxide within the fuel channel and anode.**

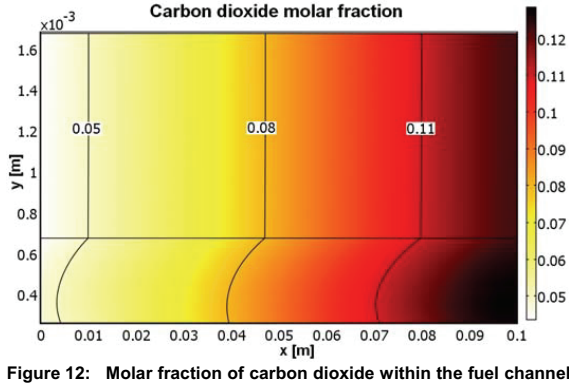


**Figure 12: Molar fraction of carbon dioxide within the fuel channel and anode.**

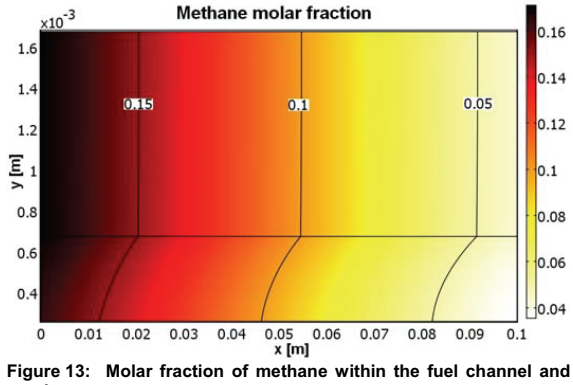


**Figure 13: Molar fraction of methane within the fuel channel and anode.**

through the anode, and the lowest mole fraction is at the TPB close to the gas outlet.

## CONCLUSIONS

In this study a SOFC CFD model (single cell anode-supported SOFC) is validated to experiments performed at NIMTE, Ningbo, China. The model contains equations for mass-, heat- and momentum transport, and chemical reactions covering internal reforming reactions and electrochemistry. The temperature distribution in the gas- and solid phase are calculated separately, according to the LTNE approach. An ionic transport distance factor to consider the distance that the oxygen ions need to be transported, from the air side to the fuel side of the cell, as well as a factor covering the active area available for electrochemical reactions divided with the x-z-cross sectional area is discussed.

The validated model is further applied to calculate the current density, molar fraction distributions as well as the different polarization losses for a case with a hydrogen-steam mixture, which is compared to a case with 30 % pre-reformed natural gas. It is concluded that the activation loss is the major of the polarization losses. The reversible open-circuit voltage is lower when pre-reformed natural gas is used as fuel, compared to the hydrogen-steam mixture.

Further development of SOFCs can enhance the transition from fossil fuels to renewable fuels. The choice of fuel for a commercial fuel cell system will depend on the available fuel infrastructure, complexity of system that is acceptable, environmental requirements to be considered and price for the different fuels etcetera.

## NOMENCLATURE

| | |
|---|---|
| $AV$ | active surface area to volume ratio, $m^2/m^3$ |
| $c_p$ | specific heat at constant pressure, J/kg/K |
| $Da$ | Darcy number, - |
| $D_{ij}$ | Maxwell-Stefan binary diffusion coefficient, $m^2/s$ |
| $D_{k,ij}$ | Knudsen diffusion coefficient, $m^2/s$ |
| $D_i^T$ | thermal diffusion coefficient, kg/(m·s) |
| $E$ | activation energy, kJ/mol, |
| $E^0$ | open circuit voltage at standard pressure, V |
| $E^{OCV}$ | reversible open circuit voltage, V |
| **F** | volume force vector, $N/m^3$ |
| F | Faraday constant, 96485 C/mol |
| $h_{s,g}$ | heat transfer coefficient, $W/(m^2K)$ |
| $h_v$ | volume heat transfer coefficient, $W/(m^3K)$ |
| $i$ | current density, $A/cm^2$ |
| $i_0$ | exchange current density, $A/cm^2$ |
| $k$ | thermal conductivity, W/m/K, reaction rate constant |
| $k''$ | pre-exponential factor, $1/(\Omega m^2)$ |
| $K$ | equilibrium constant |
| $M_j$ | molar mass of species j, kg/mol |
| $n_e$ | number of electrons transferred per reaction |
| $p$ | pressure, Pa, atm |
| $q$ | heat flux, $W/m^2$ |
| $Q$ | source term (heat), $W/m^3$ |
| R | gas constant, 8.314 J/mol/K |
| $r$ | reaction rate, $mol/(m^3s)$ |
| $S_i$ | source term (mass), $kg/(m^3s)$ |
| **T** | viscous stress tensor, $N/m^2$ |
| $T$ | temperature, K |
| u | velocity field, m/s |
| $w_i$ | mass fraction of species i, kg/kg |
| x, y, z | coordinate system, m |
| $x_j$ | molar fraction of species j, mol/mol |

### Greek symbols

| | |
|---|---|
| $\Delta S_r$ | entropy of reaction, J/K/mol |
| $\varepsilon_p$ | porosity, dimensionless |
| $\eta$ | over potential, V |
| $\kappa$ | permeability, $m^2$ |
| $\mu$ | dynamic viscosity, Pa s |
| $\rho$ | density, $kg/m^3$ |
| $\sigma$ | ionic/electronic conductivity, $\Omega^{-1}m^{-1}$ |
| $\tau$ | component thickness, m |

### Subscripts

| | |
|---|---|
| 0 | initial |
| a | anode |
| act | activation |
| b | electrode/gas channel interface |
| c | cathode |
| conc | concentration |
| e | electrode, $e \in \{a, c\}$ |
| eff | effective |
| el | electrolyte |
| g | gas phase |
| i | molecule i |
| j | molecule j |
| ohm | ohmic |
| por | porous media |
| s | solid phase |

### Abbreviations

| | |
|---|---|
| 2D | two-dimensional |
| FC | fuel cell |
| IEA | International Energy Agency |
| IT | intermediate temperature |
| MSR | methane steam reforming reaction |
| sccm | standard cubic centimeters per minute |
| SOFC | solid oxide fuel cell |
| TPB | three-phase boundary |
| WGSR | water-gas shift reforming reaction |

### Chemical

| | |
|---|---|
| $CH_4$ | methane |
| CO | carbon monoxide |
| $CO_2$ | carbon dioxide |

| | |
|---|---|
| $e^-$ | electron |
| $H_2$ | hydrogen |
| $H_2O$ | water |
| LSM | lanthanum strontium manganite |
| Ni | nickel |
| $O^{2-}$ | oxygen ion |
| $O_2$ | oxygen (gas phase molecule) |
| YSZ | yttria-stabilized zirconia |

## ACKNOWLEDGMENTS

The financial support from the Swedish Research Council (VR-621-2010-4581), the European Research Council (ERC-226238-MMFCs) and Swedish Research Links (348-2008-5999) is gratefully acknowledged. The Chinese Academy of Engineering (CAE) and the Royal Swedish Academy of Engineering Sciences (IVA) have supported the first author for a three month research visit to NIMTE, Chinese Academy of Sciences (CAS) in Ningbo, China.

## REFERENCES

[1] Staniforth J., Ormerod M., Implications for Using Biogas as a Fuel Source for Solid Oxide Fuel Cells: Internal Dry Reforming in a Small Tubular Solid Oxide Fuel Cell, *Catalysis Letter*, **81,** pp. 19-23, 2002.

[2] Andersson M., Yuan J., Sundén B., Wang W.G., LTNE Approach and Simulation for Anode-Supported SOFCs, ASME FuelCell2009-85054, Proceedings of 7th *International Fuel Cell Science, Engineering & Technology Conference*, Newport Beach, California, USA, 2009.

[3] Peksen M., Peters R., Blum L., Stolten D., Numerical Modelling and Experimental Validation of a Planar Type Pre-Reformer in SOFC Technology, *Int. J. Hyrogen Energy*, **34**, pp. 6425-6436, 2009.

[4] Andersson M., Paradis H., Yuan J., Sundén B., Modeling Analysis of Different Renewable Fuels in an Anode supported SOFC, *J. Fuel Cells*, **8**, 031013, 2011.

[5] Andersson M., 2009, SOFC Modeling Considering Mass and Heat Transfer, Fluid Flow with Internal Reforming Reactions, Licentiate Thesis, Department of Energy Sciences, Lund University, Sweden, ISSN 0282-1990.

[6] Ni M., Leung M.K.H., Leung D.Y.C., Micro-Scale Modeling of Solid Oxide Fuel Cells with Micro-structurally Grades Electrodes, *J. Power Sources*, **168**, pp. 369-378, 2007.

[7] Janardhanan V., Deutschmann O., CFD Analysis of a Solid Oxide Fuel Cell with Internal Reforming, *J. Power Sources,* **162**, pp. 1192-1202, 2006.

[8] Gorte R.J., Vohs J.M., Nanostructured Anodes for Solid Oxide Fuel Cells, *Current Opinion in Colloid & Interface Science,* **14,** pp. 236–244, 2009.

[9] Le Bars M., Worster M.G., Interfacial Conditions Between a Pure Fluid and a Porous Medium, Implications for Binary Alloy Solidification, *J. Fluid Mech.*, **550**, pp. 149-173, 2006.

[10] COMSOL Multiphysics 3.5 user guide, Stockholm, Sweden, 2008.

[11] Shi Y., Cai N., Li C., Numerical Modeling of an Anode-Supported SOFC Button Cell Considering Anodic Surface Diffusion, *J. Power Sources,* **164**, 639-648, 2007.

[12] Murzin D.Y., Salmi T., Catalytic Kinetics, Elsevier Science, 2005.

[13] Reid R.C., Prausnitz J.M., Poling B.E., The Properties of Gases & Liquids (fourth edition), McGraw-Hill Book Company, New York, USA, 1987.

[14] Yuan J., Huang Y., Sundén B., Wang W.G., Analysis of Parameter Effects on Chemical Coupled Transport Phenomena in SOFC Anodes, *Heat Mass Transfer*, **45**, pp. 471-484, 2009.

[15] Hussein M., Li X., Dincer I., Mathematical Modeling of Transport Phenomena in Porous SOFC Anodes, *Int. J. Thermal Sciences*, **46**, pp. 48-86, 2007.

[16] Suwanwarangkul R., Croiset E., Fowler M.W., Douglas P.L., Entchev E., Douglas M.A., Dusty-gas and Stefan-Maxwell Models to Predict the Concentration Overpotential of a SOFC Anode,, *J. Power Sources*, **122**, pp. 9-18, 2003.

[17] Tseronis K., Kookos I.K., Theodoropoulos C., Modeling Mass Transport in Solid Oxide Fuel Cell Anodes: A Case for a Multidimensional Dusty Gas-Based Model, *Chem. Eng. Sci.*, **63**, pp. 5626-5638, 2006.

[18] Chao C.H., Hwang A.J.J., Predictions of Phase Temperatures in a Porous Cathode of Polymer Electrolyte Fuel Cells using a Two-Equation Model,, *J. Power Sources*, **160**, pp. 1122-1130, 2006.

[19] Damm D.L., Fedorov A.G., Local Thermal Non-Equlibrium Effects in Porous Electrodes of the Hydrogen Fueled SOFC, *J. Power Sources*, **159**, pp. 1153-1157, 2006.

[20] Shah R.K., London A.L., Laminar Flow Forced Convection in Ducts. Academic Press, London, UK, 1978.

[21] Fuel Cell Handbook ($7^{th}$ edition), U.S. DoE, Morgantown, West Virginia, 2004.

[22] Winkler W., Nehter P., Thermodynamics of Fuel Cells, Fuel Cells and Hydrogen Energy, pp. 15-50, 2008.

[23] Patcharavorachot Y., Arpornwichanop A., Chuachuebsuk A., Electrochemical Study of a Planar Solid Oxide Fuel Cell: Role of Support Structures, *J. Power Sources*, **177**, pp. 254-261, 2008.

[24] Chan S.H., Low C.F., Ding O.L., Energy and Exergy Analysis of Simple Solid-Oxide Fuel-Cell Power Systems, *J. Power Sources*, **103**, pp. 188-200, 2002.

[25] Bove R. Ubertini S., Modeling Solid Oxide Fuel Cell Operation: Approaches, Techniques and Results, *J. Power Sources*, **159**, pp. 543-559, 2006.

[26] Bessler W.G., Warnatz J., Goodwin D.G., The Influence of Equilibrium Potential on the Hydrogen Oxidation Kinetics of SOFC Anodes, *Solid State Ionics*, **177**, pp. 3371-3383, 2007.

[27] Chan S.H., Khor K.A., Xia Z.T., A Complete Polarization Model of a Solid Oxide Fuel Cell and its Sensitivity to Change of Cell Component Thickness, *J. Power Sources*, **93**, pp.130-140, 2001.

 

[28] Ferguson J.R., Fiard J.M., Herbin R., 1996, Three-dimensional Numerical Simulation for Various Geometries of Solid Oxide Fuel Cells, *J. Power Sources*, **58**, pp. 109-122.

[29] Klein J.-M., Bultel Y., Georges S., Pons M., 2007, Modeling of a SOFC Fuelled by Methane: From Direct Internal Reforming to Gradual Internal Reforming, *Chem. Eng. Sci.*, **62**, pp. 1636-1649.

[30] Haberman B.A., Young J.B., 2004, Three-Dimensional Simulation of Chemically Reacting Gas Flows in the Porous Support Structure of an Integrated-Plannar Solid Oxide Fuel Cell, *Int. J. Heat and Mass Transfer*, **47**, pp. 3617-3629.

[31] Nagel F., Schildhauer T., Biollaz S., Stucki S., 2008, Charge, Mass and Heat Transfer Interactions in Solid Oxide Fuel Cells Operated with Different Fuel Gases – A Sensitivity Analysis, *J. Power Sources,* **184**, pp. 129-142.

[32] Sanchez D., Chacartegui R.,Munoz A., Sanchez T., 2008, On the Effect of Methane Internal Reforming in Solid Oxide Fuel Cells, *Int. J. Hydrogen Energy*, **33**, pp. 1834-1844.

[33] Drescher I., Lehnert W., Meusinger J., 1998, Structural Properties of SOFC Anodes and Reactivity, *Electrochimica Acta*, **43**(19-20), pp 3059-3068.

[34] Danilov V., Tade M., 2009, A CFD-Based Model of a Planar SOFC for Anode Flow Field Design, *Int. J. Hydrogen Energy*, **34**, pp. 8998-9006.

[35] Marrero-López D., Ruiz-Morales J.C. Peña-Martínez J., Canales-Vázquez J., Núñez P., 2008, Preparation of Thin Layer Material with Macroporous Microstructure for SOFC Applications, *J. Solid State Chemistry*, **181**, pp. 685-692.